CORA
Cork Open Research Archive
Cartlann Taighde Oscailte Chorcaí

Title	Improved room-temperature luminescence of core-shell InGaAs/GaAs nanopillars via lattice-matched passivation
Author(s)	Komolibus, Katarzyna; Scofield, Adam C.; Gradkowski, Kamil; Ochalski, Tomasz J.; Kim, Hyunseok; Huffaker, Diana L.; Huyet, Guillaume
Publication date	2016-02-09
Original citation	Komolibus, K., Scofield, A. C., Gradkowski, K., Ochalski, T. J., Kim, H., Huffaker, D. L. and Huyet, G. (2016) 'Improved room-temperature luminescence of core-shell InGaAs/GaAs nanopillars via lattice-matched passivation', Applied Physics Letters, 108(6), pp. 061104. doi:10.1063/1.4941435
Type of publication	Article (peer-reviewed)
Link to publisher's version	http://dx.doi.org/10.1063/1.4941435 Access to the full text of the published version may require a subscription.
Rights	**© 2016, AIP Publishing LLC. This article may be downloaded for personal use only. Any other use requires prior permission of the author and AIP Publishing. The following article appeared in Appl. Phys. Lett. 108, 061104 (2016) and may be found at http://aip.scitation.org/doi/abs/10.1063/1.4941435**
Item downloaded from	http://hdl.handle.net/10468/3691

Downloaded on 2018-08-23T18:37:49Z

University College Cork, Ireland
Coláiste na hOllscoile Corcaigh

Improved room-temperature luminescence of core-shell InGaAs/GaAs nanopillars via lattice-matched passivation

Katarzyna Komolibus, Adam C. Scofield, Kamil Gradkowski, Tomasz J. Ochalski' , Hyunseok Kim, Diana L. Huffaker, and Guillaume Huyet

Citation: Appl. Phys. Lett. **108**, 061104 (2016); doi: 10.1063/1.4941435
View online: http://dx.doi.org/10.1063/1.4941435
View Table of Contents: http://aip.scitation.org/toc/apl/108/6
Published by the American Institute of Physics

Articles you may be interested in

Nanopillar array band-edge laser cavities on silicon-on-insulator for monolithic integrated light sources
Appl. Phys. Lett. **108**, 081108081108 (2016); 10.1063/1.4942777

Ultrafast dynamics of type-II GaSb/GaAs quantum dots
Appl. Phys. Lett. **106**, 031106031106 (2015); 10.1063/1.4906106

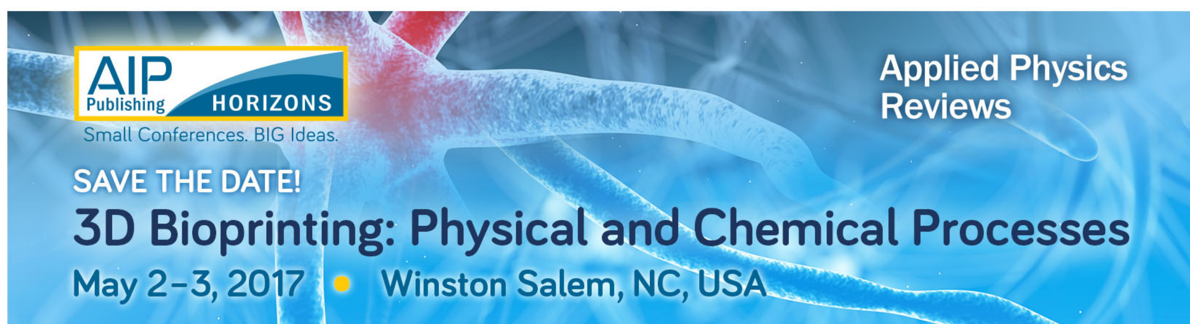

CrossMark click for updates

Improved room-temperature luminescence of core-shell InGaAs/GaAs nanopillars via lattice-matched passivation

Katarzyna Komolibus,[1,2] Adam C. Scofield,[3] Kamil Gradkowski,[1,2] Tomasz J. Ochalski,[1,2,a] Hyunseok Kim,[3] Diana L. Huffaker,[3] and Guillaume Huyet[1,2,4]
[1]*Centre for Advanced Photonics and Process Analysis, Cork Institute of Technology, Cork T12 P928, Ireland*
[2]*Tyndall National Institute, University College Cork, Cork T12 R5CP, Ireland*
[3]*Department of Electrical Engineering, California NanoSystems Institute, University of California, Los Angeles, California 90095, USA*
[4]*National Research University of Information Technologies, Mechanics and Optics, Saint Petersburg 197101, Russia*

(Received 28 October 2015; accepted 31 December 2015; published online 9 February 2016)

Optical properties of GaAs/InGaAs/GaAs nanopillars (NPs) grown on GaAs(111)B were investigated. Employment of a mask-etching technique allowed for an accurate control over the geometry of NP arrays in terms of both their diameter and separation. This work describes both the steady-state and time-resolved photoluminescence of these structures as a function of the ensemble geometry, composition of the insert, and various shell compounds. The effects of the NP geometry on a parasitic radiative recombination channel, originating from an overgrown lateral sidewall layer, are discussed. Optical characterization reveals a profound influence of the core-shell lattice mismatch on the carrier lifetime and emission quenching at room temperature. When the lattice-matching conditions are satisfied, an efficient emission from the NP arrays at room temperature and below the band-gap of silicon is observed, clearly highlighting their potential application as emitters in optical interconnects integrated with silicon platforms. © *2016 AIP Publishing LLC*.
[http://dx.doi.org/10.1063/1.4941435]

Short-distance interconnects, operating between and within silicon chips, have been a subject of intense research over the last decade. Currently, copper wires are dominant in this area; however, their large power requirements and modern increase in processing speeds make them significant bottlenecks in the data transmission chain. Switching to all-optical interconnects can help mitigate these problems, offering wide bandwidth at low cost, fJ-per-bit operating levels as well as high integration density.[1–3] Monolithic integration of efficient light sources based on III-V materials on the silicon platform presents a significant challenge but offers the best of both well-established technologies. In particular, nanopillars (NPs)[4–9]—high-aspect-ratio semiconductor nanostructures grown vertically on a substrate—are attractive candidates to facilitate this task. Their unique advantage over planar heterostructures lies in the reduced lattice-matching requirements, in that their small diameter allows for the elastic relaxation of strain in the lateral direction, and hence, even highly lattice-mismatched materials can be employed to obtain axial and radial structures.[6,10–12] Additional benefits originate from their integrability, providing the possibility for direct device engineering during the growth stage, e.g., by arranging the NP arrays into photonic crystal cavities.[13] A schematic representation of a NP-based laser coupled to a silicon on insulator (SOI) waveguide is presented in Fig. 1(a).

NPs can be either monolithic[11,14] or composed of several layers,[15,16] including barriers and an active region. While the growth of III-V NPs on a Si substrate has been previously demonstrated,[11,12] an efficient high-frequency (up to 40 Gbit/s), electrically modulated NP-based laser suitable for on-chip interconnects is still lacking. Such an emitter requires pillars of high structural quality which exhibit excellent optical properties below silicon band-gap. Recent research has focused mainly on the structural aspect of these nanostructures, with a number of research groups demonstrating the ability to grow highly uniform NPs with intentionally controlled crystal phase.[14,17] However, achieving efficient emission at room temperature (RT) remains a significant challenge due to NPs' large surface-to-volume ratio which leads to the density of surface states being a significant fraction of the total density of states in the active region. This competition is detrimental to the optical properties, as the injected carriers can be captured into surface traps and recombine non-radiatively. Consequently, in a similar manner to colloidal nanocrystals, a radial passivation layer (shell) is necessary to minimize surface recombination and improve the emission efficiency.[12,16,18] This layer should also provide lateral carrier confinement in the barrier and active regions, requiring a larger band-gap material.

This work investigates the optical properties of InGaAs/GaAs NP cores as a function of several parameters. Geometry of the NP ensemble is determined in terms of the diameter (d) and pillar spacing (pitch, p). By tuning the composition of the InGaAs active region (insert), the emission energy can be shifted below the Si band-gap. Finally, optimising the passivation by employing different shell compounds, such as GaP and AlGaAs, leads to suppression of surface states and efficient emission at RT.

The NP arrays used in this study were fabricated using a selective-area mask patterning technique. A thin SiN_x mask

[a]Author to whom correspondence should be addressed. Electronic mail: tomasz.ochalski@tyndall.ie

 © 2016 AIP Publishing LLC

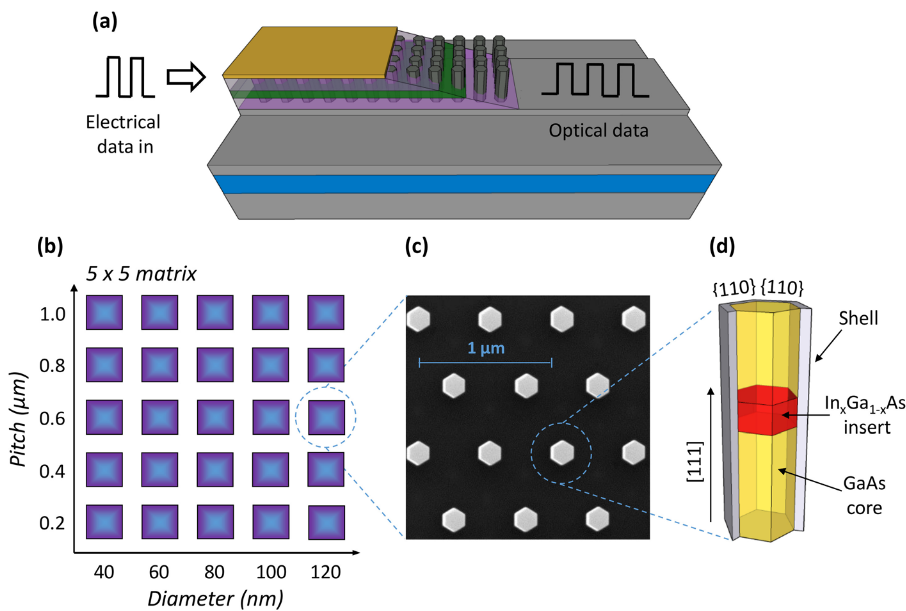

FIG. 1. (a) Schematic of proposed NP-based laser coupled to SOI waveguide, (b) Sample array schematic, (c) SEM image of NP array (d = 120 nm, p = 0.6 μm), and (d) Cross-section of a single NP.

was deposited on a GaAs(111)B substrate and subsequently patterned by e-beam lithography together with reactive ion etching to open the holes in the mask, which enables precise control of the NP geometry. This also allows for the creation of several NP arrays, typically 50 μm $\times$ 50 μm in size, on a single sample as schematically depicted in Fig. 1(b). Each array contains pillars of the same diameter and pitch, as shown in the Scanning Electron Micrograph (SEM) in Fig. 1(c). The GaAs NPs with $In_xGa_{1-x}As$ axial inserts were grown by metal-organic vapour-phase epitaxy (MOVPE). Fig. 1(d) shows a cross-section of a single NP structure. The growth is a two-step process. First, the GaAs axial core is grown at 715 °C followed by the InGaAs insert and top GaAs in a 11.5 min/3 min/7 min sequence, respectively. Subsequently, the radial shell is grown at 580 °C for 30 s. Further details of the growth process parameters can be found in Refs. 13 and 19. The NP growth rate is known to be geometry-dependent,[19] and hence the total NP height for each array varies across the sample from 600 nm up to 1.5 μm, where pillars with smaller diameter and pitch are generally taller. This implies a variation of the InGaAs insert height, which is determined from an Energy-Dispersive

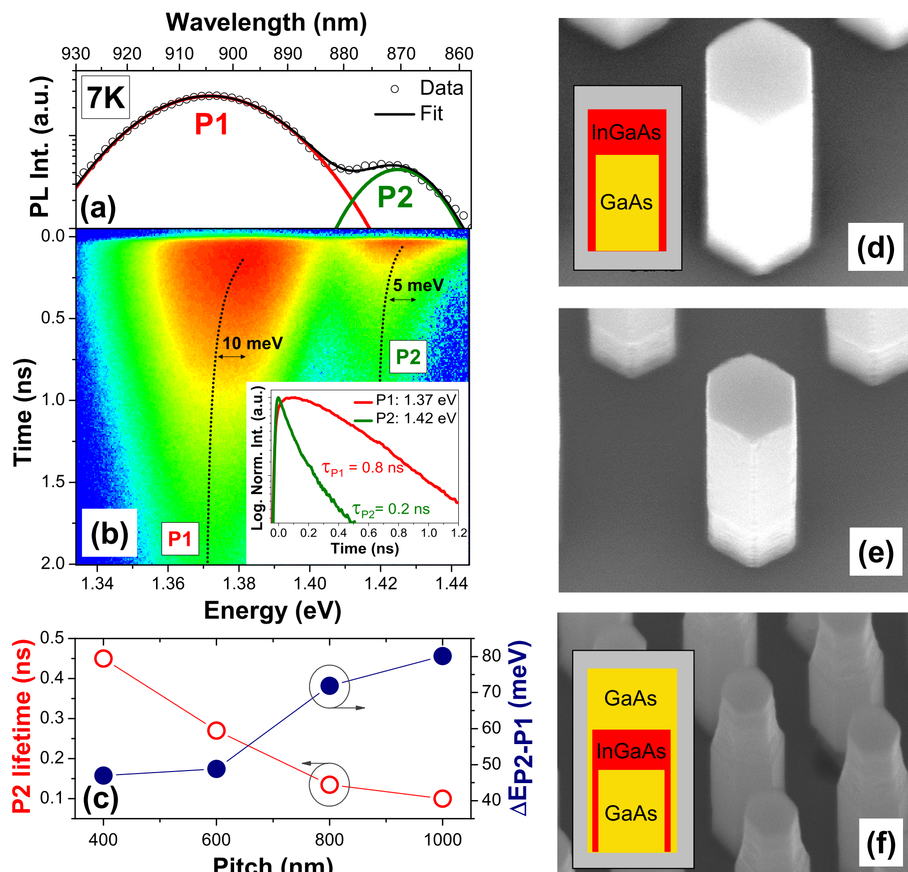

FIG. 2. (a) Emission from NP ensemble (d = 60 nm, p = 600 nm) at 7 K. Data are fitted using Gaussian peaks. (b) Streak image of the emission from the same NP ensemble at 7 K. Inset shows the decay traces for both peaks. (c) P1-P2 separation and P2 lifetime as a function of pitch for fixed d = 100 nm. (d) SEM image of GaAs/InGaAs NPs before etching. Structure depicted schematically in the inset. (e) SEM image of GaAs/InGaAs NPs after 2 min etching. (f) SEM image of a full GaAs/InGaAs/GaAs NP core structure after etching. Structure depicted schematically in the inset.

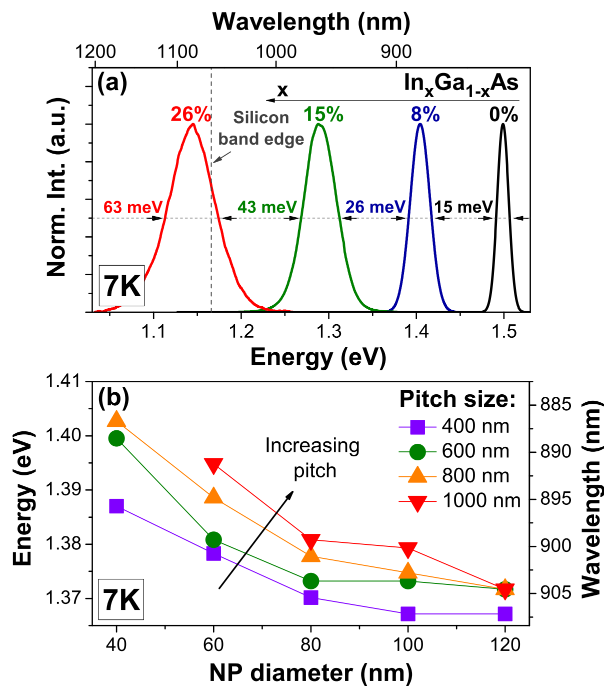

FIG. 3. PL at 7K. (a) Emission energy of P1 as a function of insert composition. Spectra originate from samples with varying In content and NP ensembles of the same geometry (p = 200 nm, d = 80 nm). (b) Emission energy of P1 as a function of NP geometry across one sample.

X-ray (EDX) scan performed along the length of the pillars to be of the order of 150–250 nm. The smallest diameter of NPs is 40 nm, which is greater that the electron de Broglie wavelength for InGaAs; therefore, the insert quantum confinement effects can be neglected. The nominal composition of the insert active region was also varied in large intervals between 0% and 26%.

A comprehensive analysis of NP optical properties and emission dynamics was performed using temperature-dependent steady-state and time-resolved photoluminescence (TRPL). The samples were placed inside a closed-cycle Helium cryostat. A Ti-Sapphire laser beam (300 fs pulses at 76 MHz), focused to a size that corresponds to the dimensions of a single NP array, was used as an excitation source. A Hamamatsu streak camera system together with 0.5-m-focal-length monochromator was used for time and wavelength-dependent detection.

Figs. 2(a) and 2(b) show a representative PL spectrum and a streak image from the ensemble of NPs measured at 7 K (explicitly shown for d = 60 nm, p = 600 nm), which can be deconvoluted into two separate Gaussian peaks. The main emission at 1.375 eV with a lifetime of 0.8 ns stems from the InGaAs insert (P1) indicating 9.7% of In concentration in the active region based on the formulas for InGaAs bandgap.[20] In addition, a side lobe at higher energies with much shorter lifetime of 0.2 ns was also observed (P2). The double feature is clearly present for all geometries for higher In concentrations. For the lowest In concentration examined, the peaks cannot be separated due to the proximity of the barrier emission.

There are several possible explanations for the origin of the P2 in the PL spectrum including an excited state, heavy-(HH) and light-hole (LH) band splitting or polytypism leading to a type-II optical transition.[14,17] However, it is tentatively attributed to the luminescence from a quantum-well-like (QW) InGaAs overgrown sidewall layer.[21,22] To assess the presence of such a layer, selective etching was performed on NP cores using an NH_4OH:H_2O_2 (1:250) solution, which gives a 10:1 GaAs/InGaAs etching ratio. Two different NP structures were investigated. The first consisting only of the bottom GaAs segment and an InGaAs insert grown on the top, while the second one being an exact replica of NP cores used in the optical studies. SEM images in Figs. 2(d) and 2(e) show the former structure before and after 2 min etching, while Fig. 2(f) presents the latter one after 1 min etching. The results reveal that while the top GaAs segment was almost entirely etched, the bottom GaAs was unaffected by the etching procedure in both cases, indicating that InGaAs shell is surrounding the bottom GaAs segment. This demonstrates the presence of a thin InGaAs layer deposited on the side walls during the growth process. Fig. 2(c) depicts the energy separation between P1 and P2, as well as P2 emission lifetime, as a function of the pitch. The energy separation was found to increase with pitch, suggesting that the QW overgrown layer becomes thinner, assuming its composition is the same as that of the insert. This thickness reduction is due to sparse arrays collecting less material decomposing on the surface of the mask.[19] Thinner QWs will have a smaller total number of states available for population by carriers. At the same time, the surface-to-volume ratio increases which, with the non-radiative recombination rate remaining constant, leads to a decrease of the emission lifetime. This means that by tuning the geometry we can eliminate this parasitic channel of radiative recombination.

Fig. 3(a) shows the dependence of the P1 emission on the insert composition. Because of the desired integrability with electronic circuits, the NP emission needs to be below

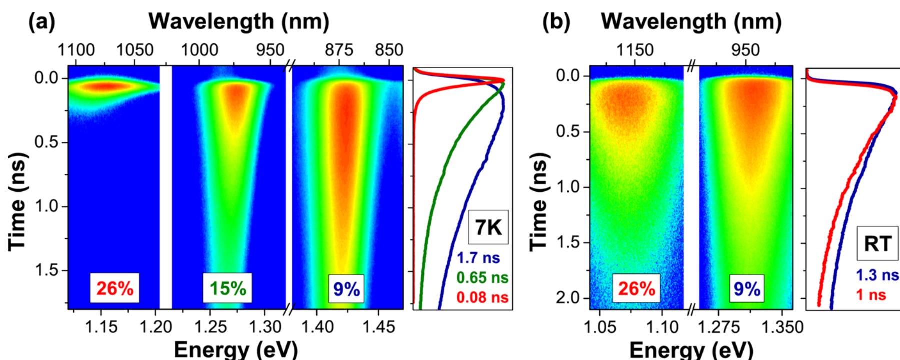

FIG. 4. TRPL of NP ensembles as a function of insert composition: (a) covered with GaP shell at 7 K (shown for p = 200 nm, d = 120 nm), (b) covered with AlGaAs shell at RT (shown for p = 800 nm, d = 120 nm).

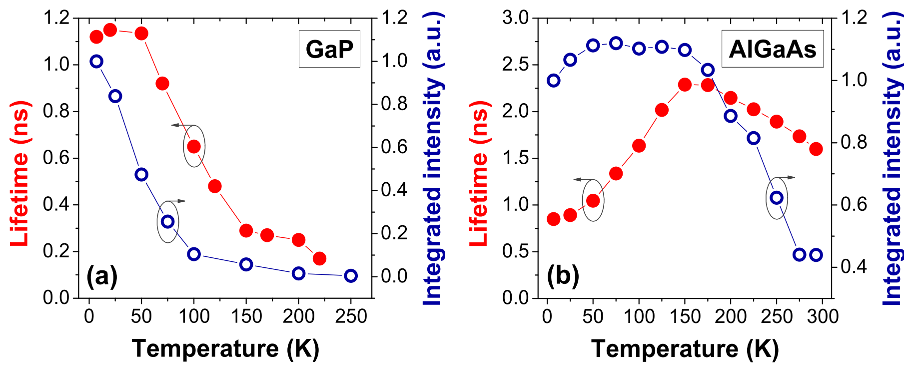

FIG. 5. Emission lifetime (closed symbols) and integrated intensity of P1 (open symbols) as a function of temperature for (a) GaP and (b) AlGaAs passivation.

the band-gap of silicon. This is fulfilled in our case by the samples containing 26% In. The full-width-at-half-maximum (FWHM) increases with concentration due to larger variations in the In incorporation into the insert across the ensemble. The composition along the NP will vary due to a variety of effects such as inhomogeneous strain distribution, lattice-pulling, and In:Ga segregation. Fig. 3(b) shows typical dependence of the P1 emission energy on NP geometry. We observe a red-shift of the order of 15–25 meV with increasing diameter and decreasing pitch. This is related to the pattern-dependent change of the In and Ga incorporation rates.[16,19] In growth species have a greater diffusion coefficient than Ga species; therefore, denser, larger nanopillars collect more material decomposing on the surface during growth, leading to a small variation in the insert composition across different arrays.

Achieving emission above the Si transparency is only one of the requirements for silicon-based devices, the other being efficient radiative recombination of carriers at RT. Fig. 4 shows TRPL images for NPs as a function of composition and shell passivation: in panel (a), the NPs were covered with GaP and in (b)—with AlGaAs. Significantly, in contrast to NP arrays covered with AlGaAs, the NP arrays with GaP passivation do not show emission at RT. Furthermore, NPs with a GaP shell exhibit rapid reduction of the carrier lifetime from 1.8 ns for 9% In in the active insert to 80 ps for 26% In. On the other hand, for AlGaAs passivation, the timescales remain at around 1 ns regardless of the insert composition. Fig. 5 presents the dependence of carrier lifetimes of P1 as a function of temperature. We can observe that for the GaP passivation (panel (a)), they decrease quickly with increasing temperature and luminescence is completely quenched around 250 K. On the other hand, the emission from AlGaAs-covered NPs (panel (b)) follows the expected free-exciton lifetime dependence $\tau \propto T^{3/2}$ up to 150 K. For higher temperatures, slight decrease of lifetime and luminescence quenching can be observed.

These phenomena are explained by taking into account the non-radiative recombination centers arising from lattice-mismatching between various components of the NP. InGaAs is normally under compressive strain when grown on GaAs. The NP geometry, specifically its small diameter, allows for this strain to be relieved in the lateral direction without the formation of defects. The growth of a tensile-mismatched GaP shell, however, results in defects forming at the core/shell interface. Their density will naturally increase with higher Indium content of the inserts, resulting in progressively larger quenching of the luminescence and shorter radiative lifetimes. Across the different arrays for each sample, we have found that the timescales vary with the local variation of insert composition, i.e., ensembles with larger diameter and smaller pitch, which have locally increased In content, have shorter lifetimes. Furthermore, with increasing temperature, more defect sites will be thermally activated, leading to a decrease in lifetimes. For temperatures above 225 K, the luminescence is completely quenched due to the overwhelming majority of carriers being captured and recombining through non-radiative means.

This does not occur for NPs with an AlGaAs shell, which is nearly perfectly matched to GaAs. Smaller lattice-mismatch at the insert/shell boundary leads to a smaller density of interface defects and up to 150 K the lifetimes increase with the emission intensity remaining constant. Above, bulk defects are thermally activated resulting in simultaneous lifetime and luminescence decrease. Worth noting is the fact that at RT emission is still ~40% as intense as at 7 K, highlighting the high crystal quality of the NPs. For applications, however, AlGaAs is not a perfect solution, since Al tends to oxidize leading to degradation in performance over time. For stable device operation, an aluminium-free shell, such as lattice-matched InGaP, is therefore required or AlGaAs can be utilized as a buffer layer for another shell in a core/shell/shell heterostructure.[18]

In summary, we have shown optical properties of InGaAs/GaAs nanopillars as a function of the active insert composition, ensemble geometry, and the passivation layer. We have achieved Si-transparent emission for 26% In composition of the insert and have shown how geometry-tuning can be used to limit the parasitic radiative channel of recombination stemming from the overgrowth layer. Finally, we have presented bright emission at RT from structures passivated with a lattice-matched shell. These structures are a major stepping stone in obtaining integrated III-V/silicon emitters that can be coupled to a Si waveguide.

This work was conducted under the Irish Government's PRTLI Cycle 5 programme, National Development Plan 2007-2013 with the assistance of the European Regional Development Fund. The authors acknowledge the support of SFI through the US-Ireland programme under Contract No. 12/US/I2490 and the NSF under Grant No. ECCS-1314253.

[1]D. A. Miller, Proc. IEEE **97**, 1166 (2009).
[2]D. A. Miller, Appl. Opt. **49**, F59 (2010).

[3]Z. Zhou, Z. Tu, T. Li, and X. Wang, J. Lightwave Technol. **33**, 928 (2015).
[4]A. Scofield, A. Lin, J. Shapiro, P. Senanayake, G. Mariani, M. Haddad, B. Liang, and D. Huffaker, Appl. Phys. Lett. **101**, 053111 (2012).
[5]J. Shieh, Y. Li, C. Ji, C. Chiu, and H. Lin, J. Renewable Sustainable Energy **7**, 033102 (2015).
[6]M. V. Nazarenko, N. V. Sibirev, K. W. Ng, F. Ren, W. S. Ko, V. G. Dubrovskii, and C. Chang-Hasnain, J. Appl. Phys. **113**, 104311 (2013).
[7]J.-R. Chang, S.-P. Chang, Y.-J. Li, Y.-J. Cheng, K.-P. Sou, J.-K. Huang, H.-C. Kuo, and C.-Y. Chang, Appl. Phys. Lett. **100**, 261103 (2012).
[8]L. Balcells, B. Martinez, O. Iglesias, J. M. García-Martín, A. Cebollada, A. García-Martín, G. Armelles, B. Sepúlveda, and Y. Alaverdyan, Appl. Phys. Lett. **94**, 062502 (2009).
[9]S. Nizamoglu, B. Guzelturk, D.-W. Jeon, I.-H. Lee, and H. V. Demir, Appl. Phys. Lett. **98**, 163108 (2011).
[10]F. Glas, Phys. Rev. B **74**, 121302 (2006).
[11]K. Tomioka, J. Motohisa, S. Hara, and T. Fukui, Nano Lett. **8**, 3475 (2008).
[12]H. Sun, F. Ren, K. W. Ng, T.-T. D. Tran, K. Li, and C. J. Chang-Hasnain, ACS Nano **8**, 6833 (2014).
[13]A. C. Scofield, S.-H. Kim, J. N. Shapiro, A. Lin, B. Liang, A. Scherer, and D. L. Huffaker, Nano Lett. **11**, 5387 (2011).
[14]P. Caroff, K. A. Dick, J. Johansson, M. Messing, K. Deppert, and L. Samuelson, Nat. Nanotechnol. **4**, 50 (2009).
[15]L. Yang, J. Motohisa, K. Tomioka, J. Takeda, T. Fukui, M. Geng, L. Jia, L. Zhang, and Y. Liu, Nanotechnology **19**, 275304 (2008).
[16]K. Hiruma, K. Tomioka, P. Mohan, L. Yang, J. Noborisaka, B. Hua, A. Hayashida, S. Fujisawa, S. Hara, J. Motohisa *et al*., J. Nanotechnol. **2012**, 169284 (2011).
[17]C. S. Jung, H. S. Kim, G. B. Jung, K. J. Gong, Y. J. Cho, S. Y. Jang, C. H. Kim, C.-W. Lee, and J. Park, J. Phys. Chem. C **115**, 7843 (2011).
[18]A. Aharoni, T. Mokari, I. Popov, and U. Banin, J. Am. Chem. Soc. **128**, 257 (2006).
[19]J. Shapiro, A. C. Scofield, A. Lin, N. Benzoni, G. Mariani, and D. L. Huffaker, preprint arXiv:1305.3581 (2013).
[20]P. Bhattacharya, *Properties of Lattice-Matched and Strained Indium Gallium Arsenide* (IET, 1993), p. 8.
[21]H. Paetzelt, V. Gottschalch, J. Bauer, G. Benndorf, and G. Wagner, J. Cryst. Growth **310**, 5093 (2008).
[22]J. Shapiro, A. Lin, D. Huffaker, and C. Ratsch, Phys. Rev. B **84**, 085322 (2011).